Thermo-Osmotic Flow in Thin Films

Andreas P. Bregulla,[1] Alois Würger,[2] Katrin Günther,[3] Michael Mertig,[3,4] and Frank Cichos[1,*]
[1]Molecular Nanophotonics Group, Institute of Experimental Physics I, University of Leipzig, 04103 Leipzig, Germany
[2]Laboratoire Ondes et Matière d'Aquitaine, Université de Bordeaux & CNRS, 33405 Talence, France
[3]BioNanotechnology and Structure Formation Group, Department of Chemistry and Food Chemistry, Chair of Physical Chemistry, Measurement and Sensor Technology, Technische Universität Dresden, 01062 Dresden, Germany
[4]Kurt-Schwabe-Institut für Mess- und Sensortechnik e.V. Meinsberg, 04736 Waldheim, Germany
(Received 21 January 2016; published 5 May 2016)

We report on the first microscale observation of the velocity field imposed by a nonuniform heat content along the solid-liquid boundary. We determine both radial and vertical velocity components of this thermo-osmotic flow field by tracking single tracer nanoparticles. The measured flow profiles are compared to an approximate analytical theory and to numerical calculations. From the measured slip velocity we deduce the thermo-osmotic coefficient for both bare glass and Pluronic F-127 covered surfaces. The value for Pluronic F-127 agrees well with Soret data for polyethylene glycol, whereas that for glass differs from literature values and indicates the complex boundary layer thermodynamics of glass-water interfaces.

DOI: 10.1103/PhysRevLett.116.188303

Osmosis is the passage of a liquid through a semipermeable membrane, towards a higher concentration of a molecular solute or salt. Osmotic processes are fundamental for life, for example in selective transport through cell membranes, and for applications such as desalination of seawater and power generation from the salinity difference with river water [1]. In physical terms, osmosis is driven by the gain in mixing entropy.

Thermo-osmosis relies on the same principle, albeit with a liquid of nonuniform *heat* content instead of a nonuniform solute concentration; accordingly, the underlying thermodynamic force is the temperature gradient rather than a concentration gradient. Since there are no heat-selective membranes, thermo-osmosis occurs in open geometries only, where heat and liquid flow in opposite directions along a solid boundary, similarly to electro-osmosis in capillaries or nanofluidic diodes [2]. Water flow due to a temperature gradient was first observed by Derjaguin and Sidorenkov through porous glass [3].

In the last decade thermal gradients have become a versatile means of manipulating colloidal dispersions, e.g., self-propulsion of metal-capped Janus particles [4,5], cluster formation through hydrodynamic interactions [6,7], force-free steering through dynamical feedback [8,9], sieving by size and stretching macromolecules [10–12], dynamical trapping of nanoparticles [13,14], and detection of DNA through functionalized gold nanoparticles (AuNPs) [15]. In all these examples, the motion arises from a superposition of thermo-osmosis and molecular osmosis [16]: The temperature gradient induces heat flow along the colloidal surface, whereas its companion fields, e.g., composition [5,17] and ion concentration [18–21], drive molecular currents. Finally, thermo-osmotic flow could be relevant for particle motion through hot nanostructures, in addition to thermophoresis and thermoconvection [22,23].

Here we report on the first microscale observation of the velocity field imposed by thermo-osmosis along the solid boundary. Both radial and vertical velocity components are determined by tracking single tracer nanoparticles. The measured flow profiles are compared to an analytical theory and to numerical calculations.

Thermo-osmotic slip velocity.—A bulk liquid in a temperature gradient reaches a nonequilibrium stationary state, with a steady nonuniform composition but zero matter flow. A solid boundary, however, exerts additional forces on the liquid; the corresponding excess specific enthalpy h in the boundary layer results in a creep flow parallel to the surface, with the effective slip velocity [24]

$$v_s = -\frac{1}{\eta}\int_0^\infty dz z h(z)\frac{\nabla T}{T} \equiv \chi\frac{\nabla T}{T}, \tag{1}$$

where η is the viscosity. An enthalpy excess, $h > 0$, leads to a negative χ and liquid flow towards the cold side, as observed for glass capillaries, clays, and silica gels [3,24], whereas a negative enthalpy $(h < 0)$ drives the liquid towards the hot side, e.g., through various synthetic membranes [25,26].

In terms of Onsager's reciprocal relations, χ is the mechanocaloric cross-coefficient, which describes equally well the excess heat carried by liquid flow at constant temperature [24]. Its explicit form can also be derived from the principles of nonequilibrium thermodynamics [27]: A solid boundary modifies the specific chemical potential μ within an interaction length λ. Plugging the thermodynamic force $-T\nabla(\mu/T)$ into Stokes' equation and using the Gibbs-Helmholtz relation $d(\mu/T)/dT = -h/T^2$, one obtains Eq. (1).

Experimental.—To measure the thermo-osmotic flow field we have constructed a sample cell that consists of two glass cover slides (Roth) enclosing a water film of about 5 μm thickness [Fig. 2(a)]. Both slides were either used untreated or covered with Pluronic F-127 (see Supplemental Material [28]). A AuNP of radius $a = 125$ nm is used as a heat source to generate a well-defined temperature gradient along the glass-water (polymer-water) interface [Eq. (2)]. The AuNP was immobilized at the upper glass surface to avoid convection.

$$T(r) = T_0 + \frac{P_{\mathrm{inc}}}{4\pi\kappa r} = T_0 + \Delta T_{\mathrm{Au}} \frac{a}{r}. \tag{2}$$

The AuNP is heated with a $\lambda = 532$ nm laser at a power of $P_{\mathrm{inc}} = 5$ mW. The temperature increment of the AuNP $\Delta T_{\mathrm{Au}} \approx 80$ K was estimated in a separate experiment [28]. Figure 1(c) displays the expected temperature profiles at the liquid-solid interface corresponding to this nanoparticle temperature at the upper slide (black curve) and the lower slide (red curve). The velocity field is measured by tracking a single AuNP of $R = 75$ nm radius. Because of its high thermal conductivity, the particle is almost isothermal and thus does not migrate in the temperature gradient. As the sample cell is thicker than the focal depth (≈ 1 μm) of the microscopy setup, the scattering intensity of the tracers varies with the z position. Selecting only the brightest particles for the analysis, for example, allows access to the velocity field close to the solid boundary.

Velocity field at the boundary.—Figures 1(a) and 1(b) give a schematic view of the velocity profile which saturates at distances beyond λ in the slip velocity v_s [Eq. (1)]. As the temperature gradient is not constant along the solid boundary one expects that the slip velocity along the upper plate decreases with the inverse square of the radius,

$$v_s = -\chi \frac{\Delta T_{\mathrm{Au}}}{T} \frac{a}{r^2}. \tag{3}$$

For $\chi > 0$ the surface flow is oriented towards the origin. A corresponding but considerably weaker surface flow (v_s') is also present at the other glass cover slide. These surface flows induce a radially symmetric volume flow $\mathbf{w}(r, z)$, which is traced by the AuNP.

In Fig. 3 the experimentally obtained velocity of the tracers close to the upper boundary of the liquid film as a function of the radial distance from the heated AuNP is plotted. The velocity profile has been measured for a bare glass plate (black curve) and one coated with Pluronic F-127 (red curve). At distances larger than 2 μm, both agree well with the power law $\propto r^{-2}$ (green dashed lines). For both systems, the flow is towards higher temperatures. The measured velocities differ by a factor of 7.5 where the larger one is found for the Pluronic F-127 coated surface. This suggests that the mobility parameter χ is considerably stronger for the nonionic block copolymer as compared to the charged glass surface. A value for v_s can be extracted when considering that the tracer velocity represents an average $\langle \mathbf{w}(r, z) \rangle_{\Delta r}$ over twice the diffusion length ($\Delta r = 620$ nm) during the exposure time (see Supplemental Material [28]). Accordingly we find a

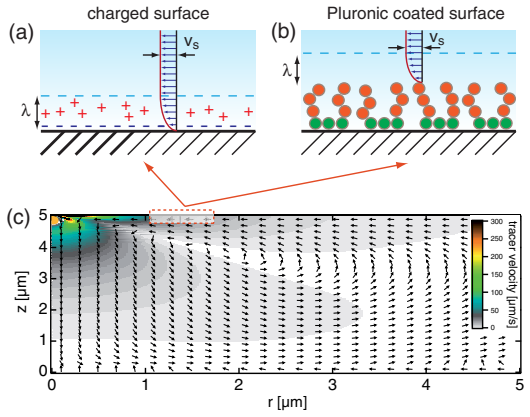

FIG. 1. Schematic view of the boundary layer at an interface with nonuniform temperature. (a) Thermo-osmotic velocity profile close to a charged solid boundary with an excess enthalpy within an interaction length λ; for $z > \lambda$ the velocity saturates at v_s. (b) The same for a Pluronic-coated surface. (c) Streamlines in the liquid film resulting from slip velocities at the upper and lower boundaries, reconstructed by numerical calculations and the experimental results for the Pluronic F-127 coated surface.

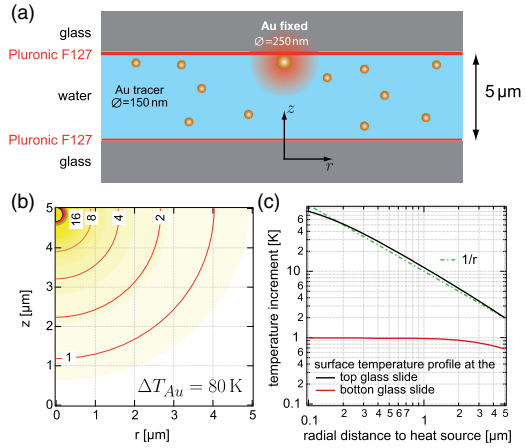

FIG. 2. (a) Principal design of the experiment. The fluid is contained between two glass cover slides in a sandwich structure with a gap of about 5 μm. A $R = 125$ nm AuNP is immobilized at the top surface and used as the heat source. A focused laser beam ($\lambda = 532$ nm) heats the particle. $R = 75$ nm AuNPs were used to measure the velocity field. (b) Temperature map around the heated AuNP in cylindrical coordinates r and z. (c) Temperature profile along the upper (black curve) and the lower glass (red curve) surface.

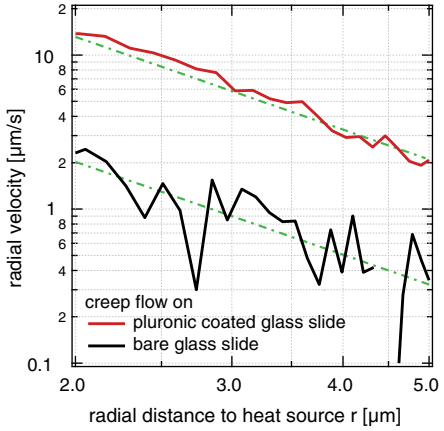

FIG. 3. Temperature profile and slip velocity along the upper boundary. The temperature agrees very well with the power law $\propto r^{-2}$. The slip velocity on both glass and Pluronic-coated glass follows this law beyond 2 microns from the heated spot.

maximum velocity of $v_s^{\text{glass}} = 40\ \mu\text{m/s}$ and $v_s^{\text{Pluronic}} = 300\ \mu\text{m/s}$

Thermo-osmotic coefficient χ.—The surface velocities and the temperature increments ΔT_{Au} yield the thermo-osmotic coefficients. Table 1 compares the coefficient χ obtained for the Pluronic coated and bare glass slides, with previously reported thermo-osmotic data and the reduced thermophoretic mobility TD_T of colloidal suspensions. For large particles the coefficients are related through $TD_T = \frac{2}{3}\chi$ [33], whereas for small particles and polymers one rather has $TD_T \simeq \chi$.

Pluronic F-127 is a nonionic triblock copolymer consisting of a central hydrophobic block of polypropylene glycol [PPG, 56 repeat units, bright green in Fig. 1(b)] and two hydrophilic blocks of polyethylene glycol (PEG, 101 units, dark red). Both molecules show complex thermodynamic behavior in water; PEG is soluble under the present conditions, whereas PPG is not [37]. Thus the PPG block is assumed to stick to the glass slides, whereas the more hydrophilic PEG parts form a molecular brush, as illustrated in Fig. 1(b). As a consequence, there is no well-defined plane of shear.

TABLE I. Thermo-osmotic parameter χ. Results are compared with data of previous work for χ and the reduced thermophoretic mobility TD_T, and with theoretical values as discussed in the main text. D_T is obtained from Soret data for polyethylene glycol [34,35] and Ludox particles [36]. The scatter of previous data is due to differences between porous glass specimens [24] and the dependence of D_T on pH and salinity [36]. We also mention that D_T of PEG depends on both molecular weight [34] and temperature [35].

χ (10^{-10} m^2/s)	This work	Theory	Prev. work	TD_T
Pluronic F-127	13	~14		15 [34,35]
Glass	1.8	~1	$-(0.2, \ldots, 1.5)$ [24]	$-(1, \ldots, 9)$ [36]

Since the water-polymer interface consists essentially of hydrophilic blocks, one expects the parameter χ to be mainly determined by the PEG properties. The excess enthalpy of PEG in water results from the balance of the hydrogen bridging of the oxygen ($h < 0$) and the opposite hydrophobic effect of the polyethylene. The measured enthalpy of mixing at low PEG content is $\Delta H = -0.66 \times 10^{-20}$ J per monomer [38]. Taking the polymer as a rod of radius b and unit length d, and assuming that the enthalpy density h is constant within the interaction length λ and zero beyond, we obtain $h = \Delta H/2\pi bd\lambda$ and a thermo-osmotic coefficient

$$\chi = -\frac{\Delta H}{\eta}\frac{\lambda}{4\pi bd} \sim 14 \times 10^{-10} \tag{4}$$

with $b = \lambda$ and the numerical value $d = 3.5$ Å. This estimate agrees well with the present measurement and previous thermophoresis data for PEG.

The situation is less clear concerning thermo-osmosis on a bare glass surface. Our experiment shows a slip velocity towards the heated spot, implying a negative enthalpy h, and the analysis of the experimental data gives $\chi = 1.8 \times 10^{-10}$ m^2/s. This sign agrees with a very recent experiment on silica Janus particles [39], whereas previous works reported the opposite effect: In their thermo-osmosis experiments on porous glass, Derjaguin *et al.* found $\chi < 0$ [40], and the Soret data of Rusconi *et al.* on Ludox particles provided a negative thermophoretic mobility D_T [36].

The excess enthalpy h in the vicinity of a glass surface is a complex quantity. Besides electrostatic and van der Waals forces, structuration of water, e.g., due to surface OH-groups, seems to play a major role [40]. The latter results in an increase of enthalpy ($h > 0$), whereas the electric-double layer contribution is negative. This would suggest that the positive coefficient χ of the present experiment results from surface charges, and that previous findings are dominated by a strong structuration contribution ($\chi < 0$). This is supported by the temperature dependence of Derjaguin's data [24]: The negative thermo-osmotic coefficient χ has a large positive derivative $d\chi/dT > 0$; this is expected for the structuration of water which is strong at low temperatures yet weakens at higher T. On the other hand, the dependence of D_T on salinity and pH reported in Ref. [36], indicates a significant electrostatic contribution, in addition to the dominant structuration effect.

The above discussion suggests that the present data ($\chi > 0$) are related to the electrostatic contribution. Glass in contact with water in general carries surface charges, which give rise to an electric double layer with Debye screening length λ, as sketched in Fig. 1. The electric-double layer enthalpy is negative and thus results in a flow towards the

heat source ($v_s < 0$). In the Debye-Hückel approximation one has $h = -\frac{1}{2}\varepsilon(\zeta/\lambda)^2 e^{-2z/\lambda}$, where ε is the permittivity and ζ the surface potential, resulting in

$$\chi = \frac{\varepsilon\zeta^2}{8\eta}. \tag{5}$$

With $\zeta \sim 30$ mV, one finds $\chi \sim 10^{-10}$ m^2/s, which agrees with both the sign and the order of magnitude of the measured value.

Bulk velocity field.—In order to fully characterize the thermo-osmotic flow field, we measured radial and vertical components w_r and w_z of the bulk velocity field $\mathbf{w}(r, z)$ and compare it to numerical simulations (COMSOL)[28]. The vertical separation is achieved by collecting signals of different intensity, which correspond to tracer particles at different z. Figure 4(a) depicts the flow field detected for the brightest tracer particles at the interface, which is directed towards the heat source. At intermediate intensities the flow is directed away from the heat source [Fig. 4(b)]. This reversal of the flow direction is obvious from the mass conservation; the inward slip velocity at the boundaries requires an outward flow in the center of the liquid film. The corresponding radial dependencies are plotted in Fig. 4(c) and agree well with the $1/r^2$ dependence of Eq. (3) at distances beyond 2 μm. At shorter distances, the velocity profile reveals a vertical component w_z. This vertical component averaged over the complete film thickness is detected by counting the number of particles which decrease or increase their scattering intensity within neighboring frames. A decrease in intensity corresponds to a downward motion of the particles, away from the heat source, while an increased intensity reveals an upward motion. Figure 4(a) depicts in the color underlay that close to the heat source particles on average move vertically away from the heat source (blue). At about $r = 2$ μm distance from the heat source a motion in the opposite direction is observed, while even farther away no net transport in the vertical direction is found. The corresponding intensity changes are plotted in Fig. 4(d). This detected vertical flow can only be due to thermo-osmosis as convection is in the used sample geometry absent. Further, the radiation pressure acting in the region of the heating laser is pointing against the detected vertical flow. The complete calculated flow field is depicted in Fig. 1(c).

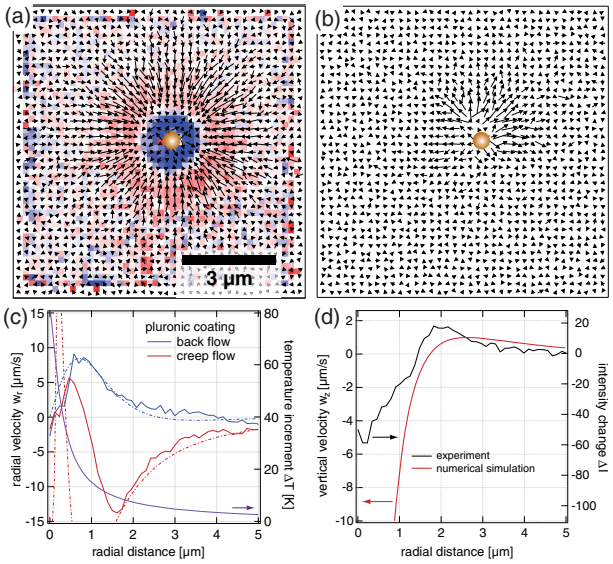

FIG. 4. (a) Two-dimensional velocity map of the tracer motion at the upper surface. The color indicates the vertical velocity with blue being a flow in the negative z direction away from the heat source and red in the positive z direction. (b) Two-dimensional velocity map of the backflow within the sample. (c) The average radial velocity at the upper surface (red curve) and the backflow (blue curve) as a function of the radial distance from the heat source. Negative velocities represent a flow towards the heat source. The dashed line displays the vertically averaged radial velocity obtained from numerical calculations. In addition, the temperature increment surrounding the heat source is displayed (purple curve). (d) The average change of the tracer intensity and the corresponding vertical velocity in comparison to the numerical calculation.

Summary.—We measured the velocity field caused by thermo-osmosis due to a heated AuNP fixed at the surface of a glass slide. The inferred interfacial flow velocities reach values of up to 300 μm/s and set up a parabolic flow field in the water film at large distances from the heat source. The slip velocities are found to be much stronger at interfaces covered with nonionic block-copolymers as compared to bare charged glass interfaces. The good agreement of the numbers gathered in Table 1 leads us to the conclusion that the slip velocity on a Pluronic-coated surface is driven by thermo-osmosis on the PEG-water interface. More generally, they confirm the role of the interaction enthalpy for the thermal separation of molecular mixtures [41] and suggest that simple models such as Eq. (4) provide a good description for the Soret data of polymers. Regarding the thermo-osmosis on a glass surface, our findings differ from previous results. The discrepancy probably results from additional contributions to the excess enthalpy, such as structuration of water or rearrangement of the hydrogen bond network, as discussed in Ref. [33]. Our results further suggest that thermo-osmotic flows along solid-liquid interfaces may contribute considerably to thermophoretic measurements in thin film geometries and may be harnessed for microfluidic applications.

The authors acknowledge financial support by Sonderforschungsbereich TRR 102, the DFG priority program 1726 "Microswimmers," the Sächsische Forschergruppe FOR 877, the DFG the joint DFG/ANR project "Thermoelectric effects at the nanoscale" Grant No. ANR-13-IS04-0003 and Leibniz Program at the Universität Leipzig.

*cichos@physik.uni-leipzig.de; http://www.uni-leipzig.de/physik/mona

[1] B. E. Logan and M. Elimelech, Nature (London) **488**, 313 (2012).
[2] C. B. Picallo, S. Gravelle, L. Joly, E. Charlaix, and L. Bocquet, Phys. Rev. Lett. **111**, 244501 (2013).
[3] B. V. Derjaguin and G. P. Sidorenkov, Doklady Akad. Nauk. SSSR **32**, 622 (1941).
[4] H.-R. Jiang, N. Yoshinaga, and M. Sano, Phys. Rev. Lett. **105**, 268302 (2010).
[5] I. Buttinoni, G. Volpe, F. Kümmel, G. Volpe, and C. Bechinger, J. Phys. Condens. Matter **24**, 284129 (2012).
[6] F. M. Weinert and D. Braun, Phys. Rev. Lett. **101**, 168301 (2008).
[7] R. Di Leonardo, F. Ianni, and G. Ruocco, Langmuir **25**, 4247 (2009).
[8] B. Qian, D. Montiel, A. Bregulla, F. Cichos, and H. Yang, Chem. Sci. **4**, 1420 (2013).
[9] A. Bregulla, H. Yang, and F. Cichos, ACS Nano **8**, 6542 (2014).
[10] S. Duhr and D. Braun, Phys. Rev. Lett. **97**, 038103 (2006).
[11] Y. T. Maeda, A. Buguin, and A. Libchaber, Phys. Rev. Lett. **107**, 038301 (2011).
[12] J. N. Pedersen, C. J. Luscher, R. Marie, L. H. Thamdrup, A. Kristensen, and H. Flyvbjerg, Phys. Rev. Lett. **113**, 268301 (2014).
[13] M. Braun and F. Cichos, ACS Nano **7**, 11200 (2013).
[14] M. Braun, A. Bregulla, K. Günther, M. Mertig, and F. Cichos, Nano Lett. **15**, 5499 (2015).
[15] L.-H. Yu and Y.-F. Chen, Anal. Chem. **87**, 2845 (2015).
[16] A. Würger, Rep. Prog. Phys. **73**, 126601(2010).
[17] A. Würger, Phys. Rev. Lett. **115**, 188304 (2015).
[18] K. A. Eslahian, A. Majee, M. Maskos, and A. Würger, Soft Matter **10**, 1931 (2014).
[19] D. Vigolo, S. Buzzaccaro, and R. Piazza, Langmuir **26**, 7792 (2010).
[20] A. Brown and W. Poon, Soft Matter **10**, 4016 (2014).
[21] M. Reichl, M. Herzog, A. Götz, and D. Braun, Phys. Rev. Lett. **112**, 198101 (2014).
[22] J. Chen, Z. Kang, S. K. Kong, and H.-P. Ho, Opt. Lett. **40**, 3926 (2015).
[23] A. Cuche, A. Canaguier-Durand, E. Devaux, J. A. Hutchison, C. Genet, and T. W. Ebbesen, Nano Lett. **13**, 4230 (2013).
[24] B. V. Derjaguin, N. V. Churaev, and V. M. Muller, *Surface Forces* (Plenum, New York, 1987).
[25] J. P. G. Villaluenga, B. Seoane, V. M. Barragán, and C. Ruiz-Bauzá, J. Membr. Sci. **274**, 116 (2006).
[26] S. Kim and M. M. Mench, J. Membr. Sci. **328**, 113 (2009).
[27] S. R. de Groot and P. Mazur, *Non-equlibrium Thermodynamics* (North Holland Publishing, Amsterdam, 1962).
[28] See Supplemental Material at http://link.aps.org/supplemental/10.1103/PhysRevLett.116.188303 for details on sample preparation, the experimental setup, an analytic flow field calculation as well as supporting experiments and an example movie from the experiments, which includes Refs. [28–31].
[29] R. G. Horn, J. Phys. (Les Ulis, Fr.) **39**, 105 (1978).
[30] M. Marinelli, F. Mercuri, U. Zammit, and F. Scudieri, Phys. Rev. E **58**, 5860 (1998).
[31] T. Sakai and P. Alexandridis, J. Phys. Chem. B **109**, 7766 (2005).
[32] M. R. Nejadnik, A. L. J. Olsson, P. K. Sharma, H. C. van der Mei, W. Norde, and H. J. Busscher, Langmuir **25**, 6245 (2009).
[33] J. L. Anderson, Annu. Rev. Fluid Mech. **21**, 61 (1989).
[34] J. Chan, J. Popov, S. Kolisnek-Kehl, and D. Leaist, J. Solution Chem. **32**, 197 (2003).
[35] R. Kita, S. Wiegand, and J. Luettmer-Strathmann, J. Chem. Phys. **121**, 3874 (2004).
[36] R. Rusconi, L. Isa, and R. Piazza, J. Opt. Soc. Am. B **21**, 605 (2004).
[37] R. Kjellander and E. Florin, J. Chem. Soc., Faraday Trans. 1 **24**, 2053 (1981).
[38] G. N. Malcolm and J. S. Rowlinson, Trans. Faraday Soc. **53**, 921 (1957).
[39] S. Nedev, S. Carretero-Palacios, P. Kühler, T. Lohmüller, A. S. Alexander, L. J. E. Anderson, and J. Feldmann, ACS Photonics **2**, 491 (2015).
[40] B. V. Derjaguin, Pure Appl. Chem. **52**, 1163 (1980).
[41] A. Würger, J. Phys. Condens. Matter **26**, 035105 (2014).